PROBING THE IGM/GALAXY CONNECTION TOWARD PKS0405-123 III: THE GALAXY SURVEY AND CORRELATIONS WITH O VI ABSORBERS

JASON X. PROCHASKA[1], BENJAMIN J. WEINER[2], HSIAO-WEN CHEN[3], AND JOHN S. MULCHAEY[4]
Accepted to ApJ: January 30, 2006

ABSTRACT

We present a galaxy survey of the field surrounding PKS0405–123 performed with the WFCCD spectrometer at Las Campanas Observatory. The survey is comprised of two datasets: (1) a greater than 95% complete survey to $R = 20$ mag of the field centered on PKS0405–123 with $10'$ radius ($L \approx 0.1L_*$ and radius of 1 Mpc at $z = 0.1$); and (2) a set of four discontiguous (i.e. non-overlapping), flanking fields covering $\approx 1\square°$ area with completeness $\approx 90\%$ to $R = 19.5$ mag. With these datasets, one can examine the local and large-scale galactic environment of the absorption systems identified toward PKS0405–123. In this paper, we focus on the O VI systems analyzed in Paper I. The results suggest that this gas arises in a diverse set of galactic environments including the halos of individual galaxies, galaxy groups, filamentary-like structures, and also regions devoid of luminous galaxies. In this small sample, there are no obvious trends between galactic environment and the physical properties of the gas. Furthermore, we find similar results for a set of absorption systems with comparable $N_{\rm HI}$ but no detectable metal-lines. The observations indicate that metals are distributed throughout a wide range of environments in the local universe. Future papers in this series will address the distribution of galactic environments associated with metal-line systems and the Lyα forest based on data for over 10 additional fields. All of the data presented in this paper is made public at a dedicated web site.

Subject headings: quasars : absorption lines

1. INTRODUCTION

Since the discovery of quasar absorption line (QAL) systems, establishing and defining their relationship to known galaxies has been a central area of research. Unfortunately, this pursuit has been hampered by a number of factors. The majority of QAL systems are identified in optical quasar spectra at $z > 2$ where galaxies have very faint apparent magnitudes. Furthermore, the glare of the background quasar prohibits imaging and spectroscopy at small angular radii. At $z \gtrsim 1$, authors have had modest success by studying Mg II absorbers, metal-line systems selected by the doublet feature at rest-frame wavelengths $\lambda = 2796$ and 2803 Å that are observable to redshift as low as $z = 0.2$ in optical spectroscopic surveys. The few studies to date associate the strongest systems with the halos of $\approx L_*$ galaxies at $z \sim 1$ (Bergeron 1988; Lanzetta 1993; Steidel 1993). Even at these redshifts, however, it is difficult to conduct large surveys to sub-L_* luminosity to trace the galactic environment of this specific class of QAL systems.

With the advance of UV spectroscopy on space-borne facilities, such as the *Hubble Space Telescope*, QAL studies have been carried out on a growing sample of low redshift AGN and quasars. To date, the majority of studies at $z < 1$ have focused on the nature of strong Lyα-forest absorbers of neutral hydrogen column density $\log N_{\rm HI} \geq 14$ (e.g. Morris et al. 1993; Lanzetta et al. 1996; Jannuzi et al. 1998) and some authors have also pushed the study to weak absorbers of $\log N_{\rm HI} = 12 - 13.5$ along several lines

of sight (Impey, Petry, & Flint 1999; Penton, Stocke, & Shull 2002, 2004). Together these results show that on large-scales (~ 1 Mpc) strong Lyα absorbers are not distributed randomly with respect to known galaxies, while weak absorbers are, exhibiting little/no trace of large-scale galactic structure (see also Grogin & Geller 1998; Tripp et al. 1998; Bowen, Pettini, & Blades 2002; Chen et al. 2005).

In addition, comprehensive surveys of galaxies and metal-line absorbers along common lines of sight have examined the correlation between galaxies and C IV systems with rest equivalent width $W_\lambda \gtrsim 0.3$Å (Chen, Lanzetta, & Webb 2001). Chen, Lanzetta, & Webb (2001) showed that nearly all galaxies found at impact parameter $\rho \leq 100h^{-1}$ kpc show associated C IV absorption while those at larger ρ rarely do. The authors interpreted this signature as a metal-enriched gaseous envelope surrounding galaxies, i.e. the absorption is galactic as opposed to intergalactic. This interpretation was further supported by an apparent correlation between the galaxy luminosity and C IV equivalent width. It is worth noting that Adelberger et al. (2003) have reported a similar correlation between C IV absorption and luminous Lyman break galaxies at $z \sim 3$. Furthermore, they describe a 'halo' with physical radius $\rho \approx 125$ kpc (perhaps the result of starburst winds) in good agreement with the Chen, Lanzetta, & Webb (2001) result. It remains an open question as to whether this pair of results are a coincidence, a generic characteristic of luminous galaxies, or even an indication of passive evolution in galactic halos from $z = 3$ to low redshift.

More recently, high resolution spectroscopy carried out at mid- and far-ultraviolet wavelengths using the *Far Ultraviolet Spectroscopic Explorer* (FUSE) and the Space Telescope Imaging Spectrograph (STIS) on board HST has offered a unique avenue to study highly ionized gas at low redshifts based on observations of O VI $\lambda\lambda 1031,1037$ (e.g.

[1] UCO/Lick Observatory; University of California, Santa Cruz; Santa Cruz, CA 95064; xavier@ucolick.org

[2] Department of Astronomy; University of Maryland; College Park, MD 20742-2421; bjw@astro.umd.edu

[3] Department of Astronomy; University of Chicago; 5640 S. Ellis Ave., Chicago, IL 60637; hchen@oddjob.uchicago.edu

[4] Observatories of the Carnegie Institution of Washington, 213 Santa Barbara St., Pasadena, CA 91101; mulchaey@ociw.edu

Savage et al. 1998; Tripp et al. 2000; Savage et al. 2002). Several authors have examined the galactic environment of O VI absorbers along the sightlines to PG1211+143 at $z_{QSO} = 0.081$ and PG1116+215 at $z_{QSO} = 0.177$ (Tumlinson et al. 2005; Sembach et al. 2004). The results show that O VI absorbers are correlated with large-scale galaxy distributions, but there is no clear evidence to support an immediate connection to individual galactic halos.

In this paper, we present optical spectra for ~ 500 objects in the field surrounding the quasar PKS0405−123. In Paper I (Prochaska et al. 2004), we analyzed the UV spectroscopy of this sightline obtained with FUSE and STIS. We focused primarily on the metal-line systems toward PKS0405−123, their ionization state and physical properties. In Paper II (Chen et al. 2005), we focused on the cross-correlation between galaxies and the Lyα forest along the sightline (see also Williger et al. 2006). In this paper, we examine the galactic environment of metal-line systems, a principal goal of the full survey. These systems are of particular interest at present, because the O VI transition provides the most efficient means of probing warm-hot ($T \sim 10^{5-7}$K) ionized gas in the intergalactic medium[5] (the so-called WHIM; Tripp et al. 2000; Danforth & Shull 2005). Numerical simulations of the low redshift universe suggest the WHIM is a major reservoir of baryons, which can be directly tested using the O VI absorbers (Cen & Ostriker 1999; Davé et al. 2001). This paper represents our group's first step toward understanding the physical environment of low-redshift O VI systems.

Unless otherwise indicated, all distances in this paper are physical separations derived from the angular diameter distance, assuming a ΛCDM cosmology with $\Omega_m = 0.3, \Lambda = 0.7, H_0 = 75$kms^{-1}Mpc^{-1}. The physical separation is most meaningful for gravitationally bound systems. To obtain transverse comoving separations, the physical separation can be multiplied by (1+z). All distances quoted scale with h_{75}^{-1} with $h_{75} = H_0/75$kms^{-1}Mpc^{-1}.

2. PHOTOMETRY

To perform target selection for multi-slit spectroscopy, we imaged the field surrounding PKS0405–123 with the Swope 40″ telescope at Las Campanas Observatory. Our first set of images were acquired on UT Oct 26, 2000 with the SITe1 CCD in direct imaging mode (pixel size 0.6964″ for the 2048x2048 array). These images were centered on PKS0405–123 and covered an $\approx 20' \times 20'$ field-of-view (FOV). We obtained B and R images under photometric (but windy) conditions for total exposure times of 900s and 350s respectively. We obtained multiple exposures with a 10″ dither patter to account for bad pixels and to facilitate the construction of a super-sky flat.

The imaging data were reduced with standard IRAF tasks to subtract the overscan and bias, and to flatten the images. We then used a set of custom routines to determine integer offsets between the images and combine the individual frames weighting by signal-to-noise. Finally, we derived a photometric solution (zero point, airmass, and color terms) on the Vega scale from standard star observations taken throughout the night: $B_{ZP} = 21.54 \pm$

0.01; $B_{AM} = 0.24 \pm 0.01$; $R_{ZP} = 21.81 \pm 0.01$; $R_{AM} = 0.08 \pm 0.006$; $(B - R) = -0.03 \pm 0.002$. The $B - R$ color term is sufficiently small that we choose to ignore it in all subsequent analysis.

TABLE 1
OBJECT SUMMARY

ID	RA	DEC	R (mag)	S/G[a]	Area ($\square''$)	flg[b]	z
98	04:08:32.0	−12:17:07	18.96 ± 0.07	0.87	3.7	7	0.26016
118	04:08:31.2	−12:21:21	19.76 ± 0.07	0.88	3.4	7	0.33226
187	04:08:29.4	−12:16:55	18.45 ± 0.07	0.02	7.1	7	0.17736
221	04:08:29.0	−12:13:28	19.40 ± 0.07	0.14	4.5	7	0.34660
258	04:08:27.4	−12:22:01	18.00 ± 0.06	0.51	5.9	7	0.08193
270	04:08:27.5	−12:16:03	18.82 ± 0.07	0.18	6.7	7	0.13360
289	04:08:27.2	−12:14:12	19.80 ± 0.07	0.14	4.2	7	0.24012
312	04:08:26.9	−12:12:10	19.52 ± 0.07	0.81	4.0	7	0.51655
324	04:08:32.0	−12:07:09	19.93 ± 0.07	0.47	3.2	7	0.30934
366	04:08:25.0	−12:16:36	18.43 ± 0.07	0.97	4.6	7	0.17706

[a]Star/galaxy classifier calculated by SExtractor. Values near unity indicate a stellar-like point-spread function.
[b]This binary flag has the following code: 1: Photometry; 2: Spectrum taken; 4= Redshift determined.

Note. — [The complete version of this table is in the electronic edition of the Journal. The printed edition contains only a sample.]

Objects in the stacked R image were identified using SExtractor (v. 2.0 Bertin et al. 2002). We required a minimum detection area of 6 pixels and a detection threshold of 1.5σ above the sky RMS. We constructed segmentation maps (images which consist of those pixels associated with each galaxy identified by SExtractor) and then calculated B and R magnitudes adopting the photometric solution listed above and assigning the average airmass of the combined images. We also used SExtractor to calculate a star/galaxy classifier which is one criterion of the target selection algorithm. Table 1 lists the RA, DEC, R magnitude and error, the star/galaxy classifier, and the area in $\square''$ for each object identified by SExtractor. Note that a small fraction of these objects may be spurious (e.g. bad pixels).

We acquired additional R images of the field on the photometric nights of UT 2002 Oct 3 and 4 to expand the field-of-view to $\approx 1\square°$. Unfortunately, owing to an error in coordinates, the area imaged is discontiguous. For these observations, we used the SITe3 CCD in direct imaging mode (pixel=0.435″ on this 2048x3150 array) and acquired multiple dithered exposures at each pointing.

For this set of observations, the images were processed with a package of IDL routines developed by JXP for direct images[6]. The algorithms are similar to standard IRAF tasks yet are tailored to this specific dataset. The routines perform overscan subtraction, the construction of a super-sky flat, and the flattening of science exposures. We also used the package to derive a photometric solution for the two nights. Finally, offsets were determined for the individual exposures and the images were combined to create a stacked image for each of four pointings.

---

[5]At $T > 10^{5.5}$K, O^{+6} and O^{+7} are the dominant ions in the WHIM (e.g. Chen et al. 2003), but these ions require X-ray observations and current instrumentation limits one to only a few sightlines.

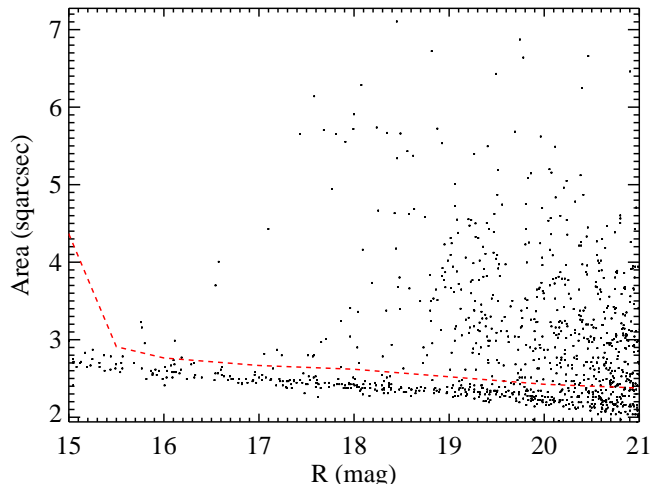[6]Publically available http://www.ucolick.org/∼xavier/IDL/index.html

FIG. 1.— Plot of the isophotal area (in square arcseconds) of all the objects within $10'$ of PKS0405–123 as a function of R magnitude. The dashed line separates the targets we pre-selects as stars and galaxies (stars are below the line). Note that the stars follow a well-defined locus to $R \approx 19.5$ mag.

3. TARGET SELECTION AND MASK DESIGN

The next task was to select objects from Table 1 for follow-up spectroscopy with the WFCCD spectrograph on the $100''$ Dupont telescope at Las Campanas Observatory. Our goal was to achieve $> 90\%$ completeness to $R \approx 20$ within a circle of $10'$ radius centered on PKS0405–123 and the same completeness to $R \approx 19.5$ for the flanking fields. For the central field, these observational parameters correspond to a luminosity $L \approx 0.1 L_*$ and radial field-of-view of 1 Mpc at $z = 0.1$. These magnitude limits represent a compromise between surveying down the luminosity function and the sensitivity limit of the WFCCD spectrograph. To distinguish stars from extragalactic sources, we examined the area of the objects as a function of magnitude (Figure 1). Point sources should occupy a uniform locus at the bottom edge of the distribution and can be removed from the target list accordingly. The line in Figure 1 represents our area-cut as a function of magnitude; objects below the line were discarded as stars with the exception of those objects where the star/galaxy classifier from SExtractor is less than 0.98. This value was adopted by comparing the full set of values against the results presented in Figure 1. Although the seeing was poorer for the imaging of the flanking fields, the smaller pixel size gives more reliable star/galaxy separation.

There are two problems with this procedure: (1) compact galaxies may be misidentified as stars; (2) galaxies and stars are not well separated at faint magnitudes. We addressed the latter concern by taking a very conservative cut at faint magnitudes. The former issue was investigated by observing a mask of objects drawn from beneath the line in Figure 1. Of the 34 targets observed, all were spectroscopically classified as stars. Nevertheless, we expect that our survey has a few percent incompleteness due to this target selection criterion, especially for objects fainter than $R = 19.5$ mag. Finally, we inspected each target galaxy to remove any erroneous objects from the SExtractor results. In a handful of cases, we removed an object

because of its proximity to a very bright star which negatively affected its photometry and isophotal area.
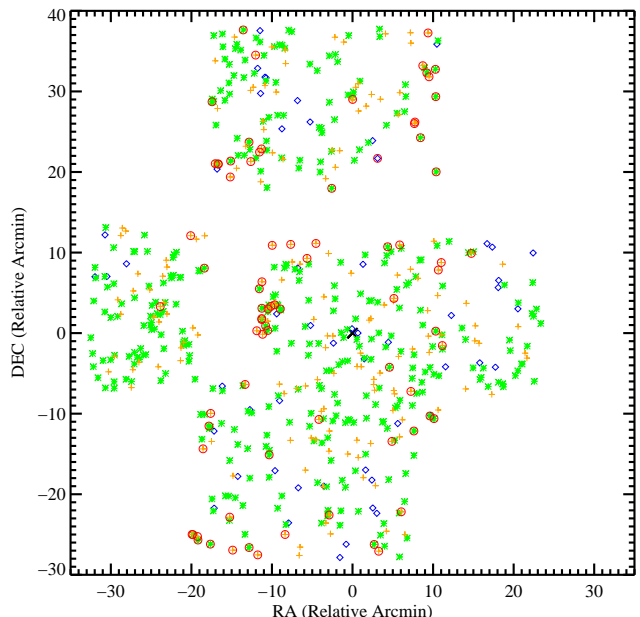

FIG. 2.— Sky position of the galaxies in the field surrounding PKS0405–123 (marked by the 'x' at RA=DEC=0). The diamonds indicate galaxies brighter than $R = 18$ mag, the asterisks are galaxies with $18 < R < 19.5$, and the plus-signs are for galaxies with $19.5 < R < 20$. The circled objects do not have a measured redshift.

In Figure 2 we show positions of all the target galaxies for the center and flanking fields. We designed 24 masks targeting 549 objects in the full field. The masks were not designed such that the slits would be observed at the parallactic angle, but we used $1.5''$ wide slits and losses due to atmospheric dispersion were not severe. The various point styles in Figure 2 identify galaxies with several magnitude ranges and the circles indicate objects with unknown redshifts. Table 1 also lists the redshift of each object and the galaxy type as defined in the next section.

4. WFCCD SPECTROSCOPY

4.1. Observations

At the time we initiated this survey, the Dupont Wide Field CCD camera (Weymann et al. 2001) was the largest field-of-view multi-slit spectrometer on any telescope. Its combination of field-of-view and throughput were essential to surveying galaxies over a large area to a sensitive luminosity limit. All of our observations were performed with brass slit masks milled at the observatory with slits covering an approximately $20' \times 15'$ field-of-view. We employed the blue grism which has a dispersion of FWHM ≈ 375 km s^{-1}.

With few exceptions, we observed each mask for two exposures totaling 1hr of integration. In the first few years

of operation, the WFCCD spectrometer suffered from significant flexure. Although the largest contribution to the flexure was fixed prior to our observations, we chose to take a coeval set of flats and arc-line calibration frames for each mask during the night, interleaved with the observations. The observations were carried out during two runs with the Dupont Telescope in Sep 2001 and Oct/Nov 2002. With little exception the nights were photometric. We used the TEK#5 CCD in each case.

For slits milled near the center of the mask, the spectral coverage spans $\lambda = 3800 - 9000$Å, with a spectral dispersion of 2Å pix^{-1} and a spatial scale of $\approx 0.75''$ pix^{-1}.

4.2. Data Reduction Pipeline

All of the spectroscopic data were reduced and analyzed with an IDL package specifically designed for the WFCCD instrument. This subsection serves as the official release of the WFCCD reduction package[7] and we will describe at greater length its procedures (for recent modifications to the package, see Geha & Blanton 2005 in prep.). Given a night of data, the user creates an IDL structure which describes the key diagnostics of each image (e.g. filter, exposure time, UT, image type, mask ID). A fraction of this information is parsed from the relatively sparse FITS header of WFCCD data and the remainder is input by the observer. After this initial step, the pipeline is fairly automated and is guided by this data structure.

The steps of the data reduction for a given mask are as follows. The dome flat exposures are scaled and combined and cosmic rays are conservatively identified in cases with multiple exposures. A sawtooth image of the flat is generated by differencing the image with itself after shifting it by a single row (spectra run parallel to the CCD rows). The resulting image exhibits a sawtooth pattern at each slit edge. Each slit edge then shows a sharp feature which is traced to determine the slit curvature and to construct a two-dimensional map of the y-distortion. The y-distortion map is used to rectify (in the spatial direction only with the sole goal of mapping the wavelength solution as noted below) the flat image and the slit edges are cross-correlated with the expected slit positions (determined from the output of the mask design software) to determine the true position of each slit. Finally, the flat for each slit is normalized by the median of the central five rows in the original (i.e. curved) frame and a final image for the normalization of pixel-to-pixel variations is created.

The pipeline then overscan subtracts and flattens the arc images associated with the mask and rectifies the frames. A one-dimensional arc spectrum is extracted down the middle of each slit and a wavelength solution is automatically derived using the known spatial coordinates of the slit as input. The dispersion of this grism spectrograph is non-linear and a 6th-order polynomial is required to achieve a fit with a typical RMS of 0.2 pixels. The pipeline then traces the curvature of the arc lines within each slit and fits a low-order polynomial to each line. It then generates a unique wavelength solution for each row in the slit, i.e. every pixel in the rectified arc image is assigned a unique wavelength. Lastly, this wavelength image is mapped back to the original data frame using the inverse of the y-distortion map.

[7]http://www.ociw.edu/lco/dupont/instruments/manuals/wfccd/redux

The remainder of the data reduction is carried out on the science images without rectification. Each exposure is overscan subtracted and flattened, a variance array is constructed assuming Poisson statistics and the read noise (5.6 electrons for gain=1), and the wavelength image of the arc closest in UT is assigned to the exposure. If two or more science exposures were obtained (without dithering along the slits), cosmic rays are masked using a conservative algorithm to avoid mis-identifying sharp emission line features. The pipeline then identifies all objects with significant flux in each slit. By default, the algorithm searches for peaks in the flux along the slit at $\lambda = 5500$Å. If a peak is identified within 5 pixels of the expected position of the science object, it is assigned as the primary object. If no object is identified within 5 pixels of the expected position, the program gives the primary object a centroid corresponding to the expected position. Any additional objects are flagged as serendipitous. The code then masks the regions surrounding all identified objects and the centroids will be used as starting points for tracing and extraction. A GUI is launched to allow the user to verify object identification and to modify the regions of the slit used to perform sky subtraction. The object centroids are saved within an IDL structure for each science exposure.
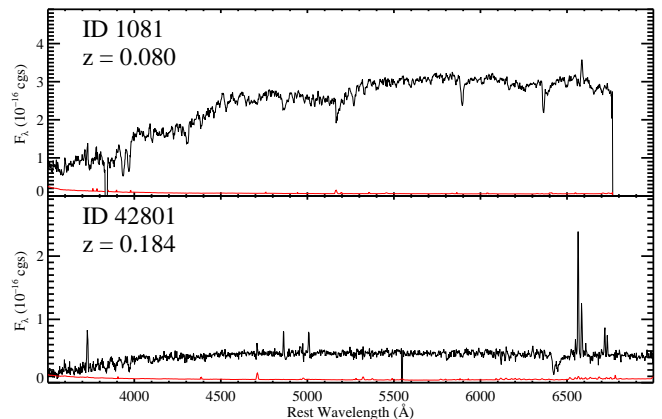

Fig. 3.— Example galaxy spectra for two of the brighter galaxies in the survey. The drop-off in flux of galaxy 1081 at $\lambda \approx 6770$Å is due to the CCD edge. Also, the feature at $\lambda \approx 3820$Å is due to a series of bad columns on the CCD. The red line traces the 1σ error array.

Sky subtraction is performed by fitting those pixels within a given slit that were not masked as object pixels. The wavelength and flux values for each unmasked pixel in the slit are used to estimate the sky spectrum. The values are fit with a third order b-spline with breakpoints centered on every other column. The b-spline is then evaluated at every pixel in the slit and subtracted. The routine iterates over all slits and the full sky subtracted image is appended to the processed data FITS file. Finally, the objects are extracted using boxcar extraction. The spatial profile is fit with a spline and an aperture containing 95% of the flux is defined. This profile is also used to flag cosmic rays within the extraction window. These pixels are flagged and their corresponding 1D spectral regions are masked (e.g. given zero weight). The 1D spectra of individual exposures is scaled and combined with optimal weighting. The routine flags and rejects additional bad pixels for masks with

two or more coeval exposures. The final 1D spectra are fluxed with a fixed sensitivity function. The sensitivity function is valid for the majority of slits but does not account for vignetting at the edges of the CCD. Figure 3 presents the spectra of two relatively bright galaxies from our sample. All of the spectra and fits tables are available at http://www.ucolick.org/~xavier/WFCCDOVI/.

4.3. Galaxy Redshifts, Completeness, and Selection Functions

An initial redshift for every extracted object was calculated with an automated procedure based on the Sloan Digital Sky Survey (SDSS) software routine *zfind*. We first smoothed and rebinned the four SDSS galaxy and star eigenfunctions (EigenGal-52223, EigenStar-52374) to the WFCCD resolution and wavelength range. We then implemented a slightly modified version of *zfind* which allows for greater freedom in the continuum of the galaxy due to poor fluxing of the WFCCD data (in particular those galaxies grossly affected by vignetting). The algorithm steps from $z = 0.05$ to 0.5 in steps of the extracted pixel width (100 km/s). At each step it fits a linear combination of the galaxy eigenfunctions to the pixel data and variance by minimizing χ^2. It then finds the minimum of the array of $\chi^2(z)$ and fits a curve to the array near the minimum to yield a redshift with formal 1 sigma uncertainty of $\sim 30 \mathrm{km\ s^{-1}}$ for the majority of spectra. We expect that systematic uncertainty (e.g. limitations of the eigenspectra) are smaller than the statistical error. Finally, the spectrum and best-fit were visually inspected by two authors and the redshift was corrected for $\approx 10\%$ of the objects. In these cases, we reapplied the automated algorithm to find the minimum χ^2 in a restricted redshift interval. The redshift values are listed in column 8 of Table 1.
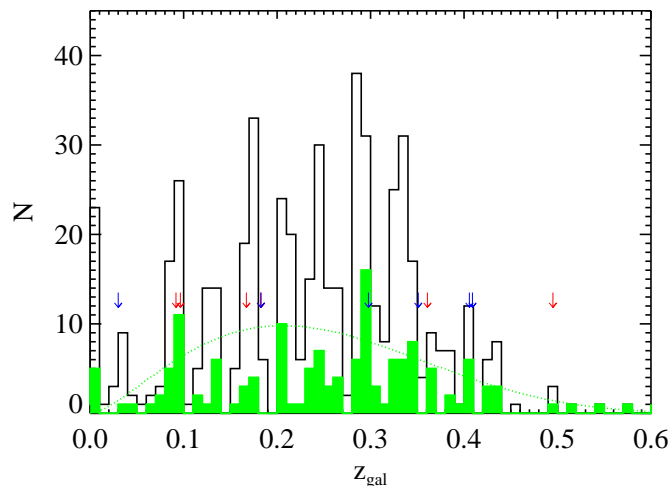

FIG. 4.— Histogram of the galaxy redshifts for the field surrounding PKS0405–123. The solid histogram shows the results for galaxies within 10′ of PKS0405–123 while the open histogram shows the distribution for our full sample. The red arrows indicate the redshifts of metal-line systems along the sightline. The blue arrows denote absorption systems with $N_{\mathrm{HI}} > 10^{14}\ \mathrm{cm^{-2}}$ but no apparent metal absorption. The objects in the bin at $z = 0$ are stars.

Figure 4 presents histograms of the redshifts for all of

the primary objects in the sample. The solid bars are the histograms for galaxies within 10′ of PKS0405–123 and the open histogram shows the full sample. Overplotted on the histograms is the selection functions for the survey (i.e. the predicted redshift distribution based on the survey limit; see Paper II for details).

In Figure 5, we report the completeness of the survey as a function of impact parameter for several magnitude limits. For the inner 10′ the curves simply indicate the fraction of galaxies with measured redshifts that are brighter than the magnitude limit. At larger impact parameter, we use the observed surface density within the inner 10′ to predict the number of galaxies and calculate the ratio of galaxies with measured redshift versus the predicted number of galaxies. Note that none of the calculations account for a incompleteness due to our star/galaxy algorithm. We believe we are overestimating the completeness by a few percent for $R > 19.5\,\mathrm{mag}$.
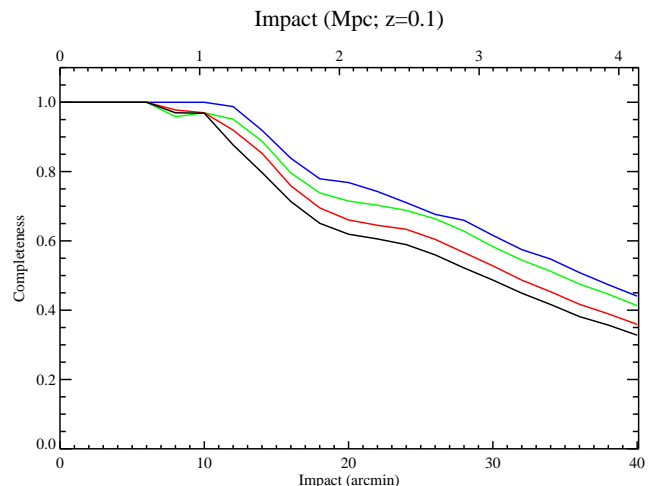

FIG. 5.— Completeness curves for the galaxy survey as a function of impact parameter to the quasar. The curves refer to limiting magnitudes $R_{lim} = 18, 19, 19.5, 20\,\mathrm{mag}$. The measurement is a direct evaluation for galaxies within 10′ of the quasar. At radii greater than 10′, the incompleteness is primarily due to the discontiguous coverage of the flanking fields (Figure 2). At these radii, we used the surface density of objects within 10′ to estimate the incompleteness in the discontiguous regions.

4.4. Galaxy Types

The eigenfunction coefficients (which are independent of galaxy brightness) from the best-fit redshift solution can be used to crudely assign a galaxy spectral type. Although the four SDSS galaxy eigenfunctions are non-physical (e.g. functions three and four include 'negative' emission lines), the first eigenfunction is dominated by absorption features and the second eigenfunction has significant Hα, [O II], and other strong emission lines. Therefore, we defined an 'early-type' coefficient E_C equal to the eigenvalue for the first eigenfunction (maximum value of 1) and a 'late-type' coefficient L_C which is the second eigenvalue minus the sum of the third and fourth coefficients. This definition was determined by examining the eigenvalues for a subset of the emission-line galaxies. The functions described by these two coefficients are orthogonal but it is possible for a
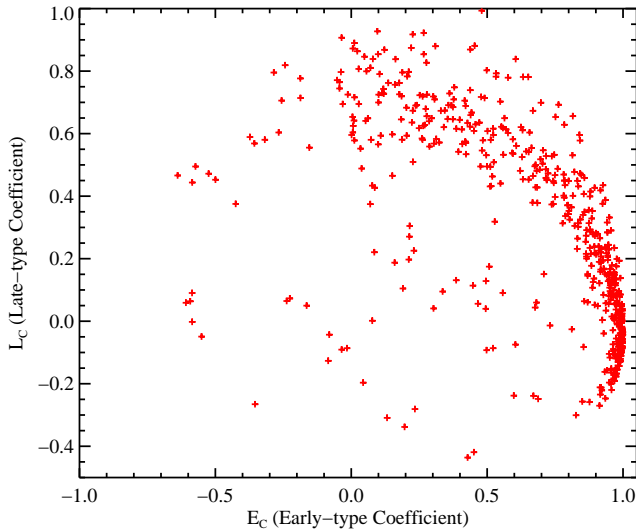
FIG. 6.— Scatter plot of the early and late-type coefficients, defined as described in the text. With a few exceptions, the galaxies follow a well-defined locus. The majority of outliers are either quasars or galaxies at very high redshift where we have limited data for spectral typing.

galaxy spectrum to have non-negligible values for both E_C and L_C. Figure 6 presents the values for all of the galaxies observed in the PKS0405−123 field. In general, the galaxies lie along a well-defined locus although there are notable exceptions. These are primarily quasars or high z galaxies with minimal coverage of the key spectroscopic features. In the following, we will distinguish early-type galaxies as galaxies with $E_C > 0.8$ and $L_C < 0.4$ and late-type galaxies with $L_C > 0.4$ and $E_C < 0.8$.

5. RESULTS AND DISCUSSION

In this section we discuss the results of our galaxy survey in terms of the origin of low z metal-line systems. For each known metal-line absorber, we examine the luminosity range, projected distances, and number density of the surrounding galaxies over a large volume to the magnitude limit defined in our redshift survey. This is different but complementary to the approach adopted by Chen, Lanzetta, & Webb (2001), who investigated the presence/absence of metal absorbers for each known galaxy at small projected distance to the sightline.

5.1. Individual Metal-Line Systems

We begin with a discussion of the galaxies associated with each of the metal-line systems identified along the sightline to PKS0405−123 (Paper I). We focus our attention on the galaxies with smallest impact parameters and also any large-scale structures identified in our survey. Table 2 lists the properties of the galaxies identified with $|\delta v| < 1000$ km s^{-1} where

$$\delta v \equiv c \frac{(z_{abs} - z_{gal})}{(1 + z_{abs})} \quad . \tag{1}$$

This velocity limit is somewhat arbitrary. We chose the value because it characterizes the peculiar velocities of

galaxies in the largest, gravitationally bound structures. We will, however, primarily focus on galaxies with $|\delta v| < 500$ km s^{-1} which are more likely to be physically associated with the absorption systems. We do not impose a limit to the impact parameter for this discussion, in part because we wish to consider the role of large-scale structures (e.g. filaments).

Figure 7 presents a visual survey of the galactic environment of each absorber. For the metal-line systems, our galaxy survey covers from ≈ 3 to 10 physical Mpc in radius for $z = 0.1$ to 0.4. Therefore, the survey is not sensitive to very large-scale structures at $z \sim 0.1$, although we emphasize that environmental correlations with galactic properties appear to be dominated by the environment measured on 1 to 3 Mpc scales (e.g. Blanton et al. 2005).

Table 2 also summarizes the physical properties of the metal-line absorbers, each of which has $N_{HI} > 10^{14}$ cm^{-2}. Furthermore, all of the systems show O VI absorption except the absorber at $z = 0.3608$ where an O VI absorber is identified[8] nearby ($\delta v = 550$ km s^{-1}). These O VI systems are particularly notable because they provide the most efficient means of probing the warm-hot intergalactic medium (WHIM; Tripp et al. 2000) with current instrumentation. Numerical simulations suggest that the WHIM is a major baryonic component of the low redshift universe (Cen & Ostriker 1999; Davé et al. 2001). They describe the WHIM as a low density gas with temperature $T \approx 10^{5-7}$K which has been shock heated during the formation of large-scale filamentary structures. If this gas is metal-enriched, then it would be detectable with UV spectroscopy via the O VI transition.

5.1.1. $z = 0.0918$

Of all the metal-line absorbers identified toward PKS0405–123, the O VI system at $z = 0.0918$ shows the largest number of galaxies with $|\delta v| < 500$ km s^{-1}. It is also the lowest redshift absorber and, therefore, we probe furthest down the luminosity function. Although one identifies 14 galaxies, only one of these has an impact parameter $\rho < 1$ Mpc and even it lies at $\rho \approx 400$ kpc. This low luminosity, emission-line galaxy has a velocity offset $\delta v = -340$ km s^{-1} which is much larger than the virial velocity of the galaxy and a physical association is unlikely. There are no additional galaxies to within 1 Mpc of the quasar sightline and we emphasize that the survey completeness is greater than 95% to $R = 20$ ($L \approx L_*/10$) at this impact parameter. It is unlikely, then, that this absorber is physically associated with a galactic halo. Examining Figure 7, one identifies three 'groups' of galaxies at $z \approx 0.091$ roughly surrounding the quasar sightline. The overall impression is that this gas occurs near the intersection of several groups, perhaps related to an over-dense, large-scale structure (i.e. filament).

5.1.2. $z = 0.0965$

A strong case can made that this O VI absorber arises in an intragroup medium. First, the sightline penetrates

---

[8]Williger et al. (2006) also report the detection of an additional O VI system at $z = 0.3616$ ($\delta v = 240$ km s^{-1}). We are not convinced of the identification based on our extraction of the STIS data and do not consider it here. In any case, its existence does not bear significantly on our results.
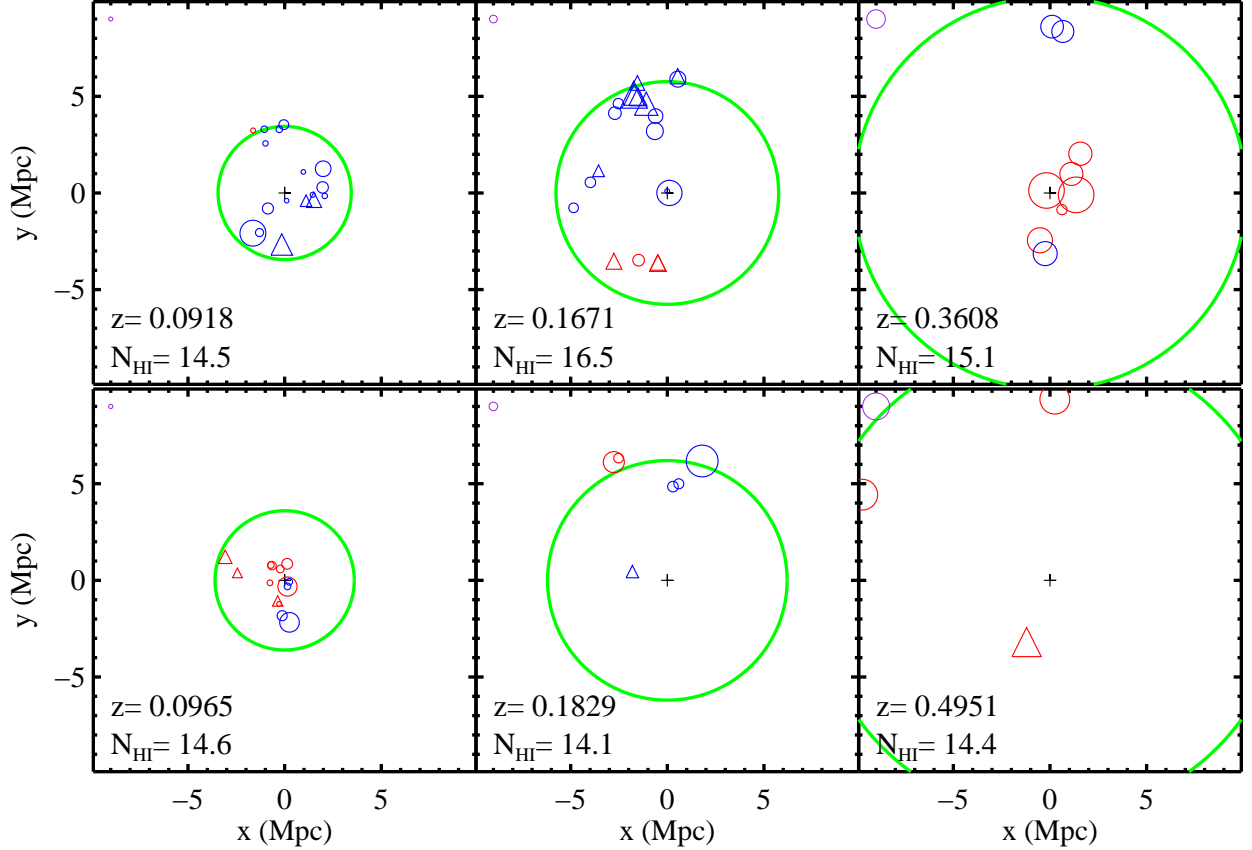
FIG. 7.— Plot of the spatial distribution of galaxies around PKS0405–123 for each of the metal-line absorption systems detected along the sightline. Galaxies are color-coded according to their velocity offset from the absorption system and circles indicate $|\delta v| < 500\,\mathrm{km\,s^{-1}}$ and triangles are for $1000 > |\delta v| > 500\,\mathrm{km\,s^{-1}}$. The size of the symbol is proportional to the luminosity of the galaxy. The purple circle in the upper-left corner of each sub-panel corresponds to $R = 20\,\mathrm{mag}$, i.e. the magnitude limit of the inner $10'$ of the survey. This corresponds to $L \approx L_*/10$ at $z = 0.1$ and $L \approx L_*$ at $z = 0.25$. The green circle in each sub-plot shows the approximate radial limit of the survey ($36'$).

a galaxy group containing several $L \gtrsim L_*$ galaxies, including three early-type galaxies. Restricting the analysis to the galaxies within $2.2\,\mathrm{Mpc}$, the group has a velocity centroid offset of $140\,\mathrm{km\,s^{-1}}$ from the gas and a velocity dispersion of $210\,\mathrm{km\,s^{-1}}$. Second, the galaxies with $|\delta v| < 500\,\mathrm{km\,s^{-1}}$ surround the sightline and the gas must be gravitationally bound to the group. Third, although there are three galaxies with $\rho = 250 - 350\,\mathrm{kpc}$, these have too low luminosity for their virial radius to encompass the sightline. In short, it is more likely the intragroup medium gives rise to this O VI absorption system (Mulchaey et al. 1996; Fukugita et al. 1998). In Paper I we estimated the volume density for this gas $n_H \approx 10^{-5}\,\mathrm{cm^{-3}}$ assuming the extragalactic ultraviolet background radiation field from Davé & Tripp (2001). The gas density profile of the intragroup medium can be estimated directly for X-ray detected groups from the X-ray surface brightness profile. For an X-ray group with central volume density $n_H \approx 10^{-3}\,\mathrm{cm^{-3}}$ and a standard beta model (i.e. Helsdon & Ponman 2000; Mulchaey et al. 2003), the density at $\rho = 100\,\mathrm{kpc}$ is $\approx 10^{-4}\,\mathrm{cm^{-3}}$. If the group at $z = 0.0965$ is not an X-ray group, one might expect a significantly lower gas density, i.e. one consistent with $10^{-5}\,\mathrm{cm^{-3}}$ (Mulchaey et al. 1996). We also note, however, that this system exhibits C III absorption and we have argued that the gas is predominantly photoionized and in a single phase (Pa-

per I). We cannot rule out, however, that the the O VI gas is in a multi-phase medium.

5.1.3. $z = 0.16710$

This partial Lyman limit system has been previously identified with two galaxies at $\rho \approx 100\,\mathrm{kpc}$ (Spinrad et al. 1993). One of these is a bright early-type galaxy and the other is a dwarf galaxy with modest emission lines. These are the only two galaxies in our survey of the PKS0405–123 field with impact parameter less than $150\,\mathrm{kpc}$. Prior to performing our survey, we expected to identify additional galaxies at the redshift of the absorber in the field surrounding the sightline. To our surprise, we find no additional galaxies at $z \approx 0.167$ with $L > 0.5L_*$ within $3\,\mathrm{Mpc}$ of the absorber. In fact, there is only one additional galaxy with $|\delta v| < 300\,\mathrm{km\,s^{-1}}$ and it lies at an impact parameter of nearly $4\,\mathrm{Mpc}$. We will return to this absorber in § 5.2.

TABLE 2

SUMMARY OF THE GALAXIES NEIGHBORING METAL-LINE ABSORPTION SYSTEMS

ID	z	R	Lum (L^*)	δv (km/s)	ρ (kpc)	E_c	L_c
$z = 0.0918$, $N_{HI} = 14.5$, $N(\mathrm{OVI}) = 13.8$, [M/H] $= > -1.4$
1698	0.0906	19.74	0.13	-341	412.4	0.49	0.04
10258	0.0899	17.72	0.87	-517	1175.1	-0.03	0.69
3386	0.0917	17.81	0.80	-24	1181.2	1.00	-0.03
10552	0.0916	19.52	0.17	-60	1455.3	0.98	0.20
11489	0.0903	19.74	0.14	-403	1457.6	0.60	-0.24
10309	0.0899	17.09	1.56	-531	1552.4	-0.52	0.47
10900	0.0912	17.74	0.85	-161	1986.0	0.05	0.64
10498	0.0908	19.35	0.19	-276	2081.1	0.95	0.07
11603	0.0908	17.06	1.59	-278	2354.3	0.97	0.14
30847	0.0902	18.49	0.43	-436	2427.6	-0.24	0.06
30799	0.0917	15.97	4.37	-21	2650.3	0.94	-0.16
30260	0.0899	16.38	2.99	-522	2669.7	0.99	-0.08
41345	0.0906	19.37	0.19	-333	2748.4	-0.02	-0.09
42607	0.0911	18.94	0.28	-206	3305.6	0.56	0.09
42613	0.0908	18.97	0.27	-263	3462.5	0.94	0.39
43005	0.0910	18.08	0.62	-226	3536.0	0.40	0.64
42509	0.0924	19.57	0.16	153	3623.5	0.50	0.13
$z = 0.0965$, $N_{HI} = 14.7$, $N(\mathrm{OVI}) = 13.7$, [M/H] $= -1.5$
1457	0.0965	19.03	0.29	-13	247.5	0.18	0.76
1602	0.0965	19.01	0.29	-4	342.7	0.21	0.27
1601	0.0967	16.74	2.39	56	350.7	0.68	0.38
2254	0.0970	18.74	0.38	149	629.9	0.67	0.46
3138	0.0980	19.38	0.21	414	770.8	0.50	-0.09
1659	0.0970	17.99	0.75	132	864.8	0.00	0.65
2973	0.0971	18.52	0.46	161	1006.3	0.48	0.49
3082	0.0973	19.06	0.28	228	1068.0	0.87	0.36
2485	0.0986	18.05	0.72	573	1123.1	0.36	0.69
32180	0.0974	19.77	0.15	244	1250.0	0.19	0.58
31271	0.0957	18.13	0.66	-222	1832.6	-0.50	0.45
30806	0.0964	16.69	2.50	-18	2186.3	0.91	0.05
21111	0.0994	18.20	0.62	797	2474.9	0.88	0.40
21834	0.1000	17.49	1.20	970	3307.2	0.95	0.15
$z = 0.1671$, $N_{HI} = 16.5$, $N(\mathrm{OVI}) = 14.8$, [M/H] $= -0.2$
90033	0.1670	21.00	0.15	-26	92.6	...	...
1753	0.1670	17.43	4.14	-15	107.8	0.65	0.45
40291	0.1659	18.30	1.86	-317	3264.4	1.00	0.04
30714	0.1710	18.49	1.56	997	3629.7	0.93	-0.04
30693	0.1708	18.32	1.83	960	3661.2	0.07	0.81
21409	0.1650	19.08	0.90	-547	3739.0	0.70	0.50
30811	0.1673	19.11	0.88	48	3782.8	0.19	0.72
21074	0.1652	19.33	0.72	-488	4019.2	0.31	0.88
41036	0.1652	18.63	1.37	-497	4025.4	1.00	-0.02
30761	0.1698	18.42	1.66	687	4487.2	0.25	0.72
41676	0.1649	17.61	3.52	-565	4747.1	0.39	0.62
20274	0.1660	19.52	0.60	-292	4910.1	0.51	0.58
41188	0.1652	18.93	1.04	-478	4942.9	0.92	0.42
42077	0.1646	18.15	2.14	-652	5207.7	1.00	0.02
41685	0.1652	19.36	0.70	-484	5272.7	0.24	0.69
42162	0.1647	17.88	2.74	-622	5354.5	0.97	-0.10
42163	0.1647	17.28	4.78	-629	5375.1	0.95	0.11
42816	0.1650	18.59	1.42	-548	5899.1	0.68	0.48
42990	0.1653	18.42	1.66	-468	5914.8	0.16	0.84
43154	0.1650	18.52	1.52	-536	6064.1	0.29	0.64
$z = 0.1829$, $N_{HI} = 14.1$, $N(\mathrm{OVI}) = 14.0$, [M/H] > -2.0
3623	0.1796	19.17	1.02	-830	1863.9	-0.29	0.80
41580	0.1819	19.54	0.73	-261	4859.0	0.42	0.69
41714	0.1823	19.67	0.65	-155	5032.4	0.19	0.10
42851	0.1822	17.14	6.61	-176	6432.7	0.80	0.34
42801	0.1842	18.04	2.87	326	6715.2	-0.19	0.71
42983	0.1834	19.74	0.60	121	6811.1	0.68	0.04

Note. — The galaxy summary is restricted to those galaxies within 1000 km s^{-1} of the absorption system. The N_{HI}, $N(\mathrm{OVI})$, and [M/H] values are taken from Paper I. The impact parameter refers to physical separation, not comoving.

TABLE 2 CONTINUED

ID	z	R	Lum (L^*)	δv (km/s)	ρ (kpc)	E_c	L_c
$z = 0.3608$, $N_{HI} = 15.1$, $N(OVI) < 13.3$, $[M/H] > -0.7$							
1967	0.3612	18.58	8.24	97	220.5	0.98	0.18
90068	0.3610	21.30	0.67	44	1062.4	...	...
1039	0.3610	18.58	8.27	47	1356.6	0.98	0.09
1236	0.3615	19.52	3.47	156	1482.2	0.98	0.02
2170	0.3609	19.34	4.11	27	2503.3	0.99	-0.08
907	0.3617	19.51	3.50	194	2567.9	0.63	0.53
32334	0.3598	19.43	3.76	-219	3147.8	0.99	-0.02
41821	0.3587	19.63	3.14	-457	8383.7	0.98	-0.07
41971	0.3598	19.56	3.35	-218	8606.8	0.99	-0.10
$z = 0.4951$, $N_{HI} = 14.4$, $N(OVI) = 14.3$, $[M/H] > -0.3$							
2496	0.4992	19.82	5.56	816	3412.7	0.94	0.23
41479	0.4961	19.78	5.76	201	9377.7	0.99	0.01
21907	0.4953	19.71	6.17	36	10679.6	0.98	0.10

Note. — The galaxy summary is restricted to those galaxies within 1000 km s^{-1} of the absorption system. The N_{HI}, $N(OVI)$, and [M/H] values are taken from Paper I. The impact parameter refers to physical separation, not comoving.

5.1.4. $z = 0.1829$

There are two Lyα absorbers at $z = 0.1825$ and $z = 0.1829$ (Williger et al. 2006) with O VI/H I ratios differing by more than an order of magnitude (Paper I). Focusing on the O VI absorber at $z = 0.1829$, we identify zero $L \approx L_*$ galaxies within 2 Mpc of the sightline and none within 5 Mpc with $|\delta v| < 800$ km s^{-1}. Although our survey limit does not preclude the presence of a sub-L_* galaxy, our results show that there is no significant galaxy group or large-scale structure associated with the gas. This observation is qualitatively different from all of the other metal-line systems toward PKS0405–123.

5.1.5. Systems with $z \approx 0.36$

There are a pair of metal-line systems at $z = 0.3608$ and $z = 0.3633$ with a velocity separation of $\delta v = 550$ km s^{-1}. The absorber at $z = 0.3608$ is notable for exhibiting several oxygen ions yet no significant O VI absorption. In contrast, the $z = 0.3633$ system exhibits O VI and likely C III gas. Our galaxy survey reveals a group of very bright, early-type galaxies coincident with the $z = 0.3608$ absorber. One may place the gas within the elliptical at $\rho = 220$ kpc (ID 1967) but more likely the gas is associated with the intragroup medium of these galaxies or a galaxy below our magnitude limit (i.e. $L < 2L_*$). In any case, this is a striking example of an over-dense galactic environment hosting a metal-line absorption system.

5.1.6. $z = 0.4951$

This strong O VI absorption system is at too high redshift to even qualitatively discuss its galactic environment based on our current survey. In passing, we note two galaxies with $|\delta v| \lesssim 200$ km s^{-1} and $L \approx 6L_*$ which are at very large impact parameter ($\rho \approx 10$ Mpc) from the quasar sightline. We also note that the Williger et al. (2006) compilation reveals no additional galaxies at fainter magnitudes closer to the sightline.
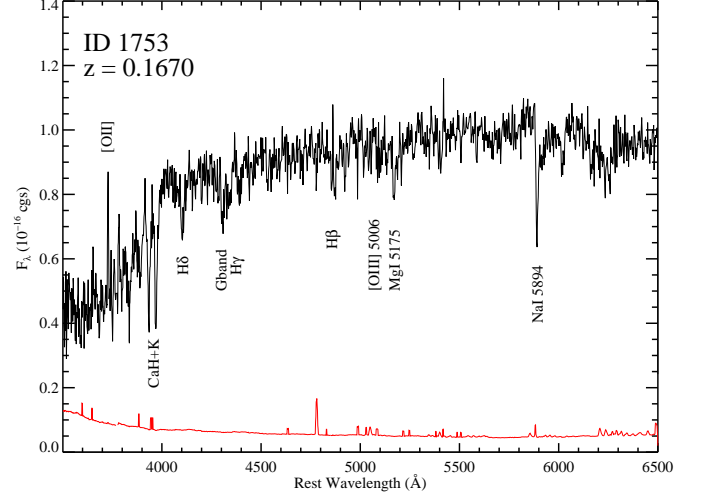

FIG. 8.— Galaxy spectrum of the likely host galaxy of the partial Lyman-limit absorption system at $z = 0.1671$ toward PKS0405–123. The Balmer features, weak [OII] emission, and absence of [O III] emission mark this galaxy as an Sb spectral type. This indicates minimal current star formation yet a significant episode of star formation over the past ~ 1 Gyr.

5.2. Halo Gas at Low Redshift

Consider further the absorption system at $z = 0.1671$. Combining our galaxy survey with the sample from Williger et al. (2006), it is apparent the system is associated with one of the two galaxies at impact parameter $\rho \approx 100$ kpc from the sightline. We consider it very unlikely that the gas is within the halo of the low luminosity galaxy because (1) the gas has nearly solar metallicity and (2) the gas is almost certainly gravitationally bound to the bright spiral given the negligible velocity separation and large stellar mass of this galaxy. In the following, therefore, we physically associate this metal-line system with the bright, early-type spiral first identified by Spinrad et al. (1993). Figure 8 shows our WFCCD spectrum of this galaxy. One identifies strong Ca H+K, G-band, and Balmer absorption lines in the spectrum and also a weak but significant [OII] emission line. The spectral type is that of an Sb galaxy (Kennicutt 1992) and the Balmer lines suggest a significant episode of star formation ≈ 1 Gyr ago.

This identification has several striking implications. First, the observations suggest a tenuous, ionized multi-phase gas within the halo of the early-type spiral. As discussed in Chen & Prochaska (2000), the absorption system exhibits two distinct phases: (1) a photoionized gas associated with Si$^+$, Si^{++}, C$^+$ ions and presumably the majority of H I gas. The temperature of this phase is a few 10^4 K. Adopting the mean extragalactic background radiation field inferred by Davé & Tripp (2001), the mean number density of the gas is $n_H = 6 \times 10^{-4}$ cm^{-3}; (2) a hot, ionized gas associated with O VI, N V, and probable S VI absorption (Paper I). It is likely this gas is collisionally ionized with temperature $T \approx 2 \times 10^5$ K. It is important to note that the photoionized gas may have characteristics similar to higher redshift Mg II absorbers. The association of this gas with the bright, early-type spiral is suggestive of the observed connection between bright spi-
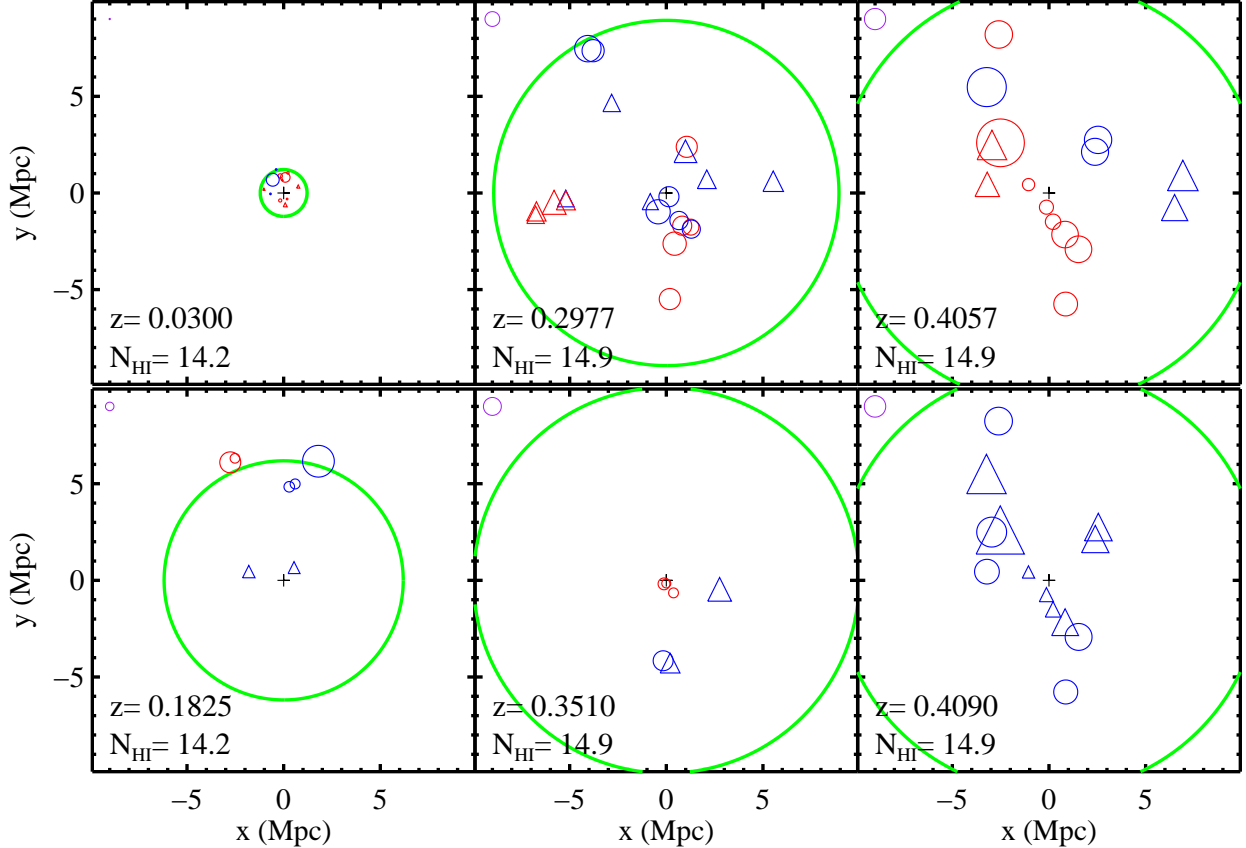
FIG. 9.— Plot of the spatial distribution of Lyα 'clouds' with $N_{\rm HI} > 10^{14}\,{\rm cm}^{-2}$ but no apparent metal-line absorption. The symbols and color coding are the same as Figure 7.

rals and Mg II absorbers at $z \sim 1$. Indeed, Spinrad et al. (1993) reported a tentative detection of the Mg II doublet and noted the resemblance between this absorber and Mg II systems (Steidel 1993). Adopting the photoionization model from Paper I, we predict $\log N({\rm C\,IV}) > 13.5$ from the low-ionization phase alone. We expect a C IV equivalent width in excess of 0.3Å, and, therefore, that this absorber would follow the results of other C IV/galaxy absorber-pairs (Chen, Lanzetta, & Webb 2001).

Second, the velocity offset between the absorber and galaxy redshift is small ($\delta v \approx -15\ {\rm km\ s}^{-1}$) suggesting the gas is bound to the galaxy. Third, it suggests a significant mass of gas in the outskirts of the galactic halo. Applying the ionization corrections derived in Paper I, we derive a total hydrogen column density $N_H = 10^{19}\,{\rm cm}^{-2}$ for the gas associated with the lower temperature phase. If we assume a constant surface density to $\rho = 100\,{\rm kpc}$ with covering fraction f, then the integrated mass is $M = f \cdot 3 \times 10^9 M_\odot$. If the surface density increases radially toward the galactic center, then the gas mass could be considerably higher even if the medium is clumped. Fourth, the gas has nearly solar metallicity: $[{\rm Si/H}] = -0.25$ dex. For this reason, it is very unlikely the gas is being accreted from the local IGM. Instead, we contend the gas was enriched within the galaxy and then expelled to large radii. This interpretation is supported by the strong Balmer absorption lines in the galaxy spectrum (Figure 8) which indicate a recent episode of star formation. Assuming a distance of 100 kpc, the gas

would only need an outflow velocity of $\sim 100\ {\rm km\ s}^{-1}$ to travel this distance in 1 Gyr.

Fifth, we emphasize that the O VI equivalent width is among the largest observed at extragalactic distances. In Chen & Prochaska (2000), we speculated that this gas may arise in an intragroup medium. The results of our galaxy survey contradict this claim. Instead, one must associate the gas with one of the two nearby galaxies. This has further implications for the multi-phase nature of the absorber. If the two phases are co-spatial, then it is very likely in pressure equilibrium with the photoionized gas embedded within the hotter, collisionally ionized O VI gas. Adopting $n_H = 6 \times 10^{-4}\,{\rm cm}^{-3}$ and $T \approx 20000\,{\rm K}$ for the photoionized phase and also $T_{hot} = 2 \times 10^5\,{\rm K}$ for the O VI phase, we derive $n_H^{hot} = 6 \times 10^{-5}\,{\rm cm}^{-3}$. As Chen & Prochaska (2000) noted, the gas must have a density on this order or lower to avoid cooling in less than a dynamical time. Therefore, a qualitatively self-consistent model can be constructed where this partial Lyman limit system is a pressure-supported photoionized 'cloud' located in a warm, collisionally ionized gas at large radii from this early-type spiral.

Sixth, adopting the n_H^{hot} density and assuming the hot phase fills the galactic halo to $r = 100\,{\rm kpc}$, we derive a hot gas mass $M^{hot} \approx 5 \times 10^9 M_\odot$. Seventh, we note that this system has the highest $N_{\rm HI}$ value along the PKS0405–123 sightline and is the only absorber unambiguously identified with a galactic halo. While Lyα 'clouds' with $N_{\rm HI} >$

<div align="center">

TABLE 3
GALACTIC ENVIRONMENT SUMMARY

</div>

z	N_{HI}	N_{OVI}	[M/H]	$\rho_{nearest}^a$ (kpc)	$L_{nearest}^a$ (L_*)	L_{lim}^b (L_*)	$\rho_{>L_*}$ (kpc)	$n_{3\mathrm{Mpc}}^c$	Comment
0.0918	14.5	> -1.4	13.8	412	0.1	0.1	2354	7(1.2)	Filament?
0.0965	14.7	-1.5	13.7	247	0.3	0.1	351	5(1.2)	Group
0.1671	16.5	-0.2	14.8	108	4.1	0.4	108	1(1.8)	Galaxy
0.1829	14.1	> -2.0	14.0	4859	0.7	0.5	6433	0(1.9)	Void?
0.3608	15.1	> -0.7	< 13.3	220	8.2	2.2	220	5(0.4)	Group
0.4951	14.4	> -0.3	14.3	9378	5.8	4.7	9378	0(0.0)	??
0.0300	14.4	< -1.5	< 13.5	360	0.0	0.0	888	2(0.8)	Group?
0.1825	14.9	< -1.5	< 13.8	4851	0.7	0.5	6421	1(1.9)	Void
0.2977	14.0	< -1.5	< 13.3	236	2.6	1.4	236	10(0.3)	Halo
0.3510	14.2	< -1.5	< 13.5	218	0.9	2.1	4163	1(0.4)	Void?
0.4057	14.9	< -2.0	< 13.6	747	1.3	2.9	747	3(0.0)	Filament?
0.4089	14.4	< -1.5	< 13.5	3242	4.0	3.0	3242	3(0.0)	Filament?

[a]Impact parameter and luminosity of the nearest galaxy to the sightline.

[b]imitting magnitude assuming R_{lim}=20mag.

[c]Number of galaxies with physical impact parameter $< 3\,\mathrm{Mpc}$, $L > \max(L_*/2, L_{lim})$, and $|\delta v| < 750\mathrm{km\,s^{-1}}$. The quantity in parenthesis is the average number using the volume of this 3 Mpc radius region and the luminosity limit and also adopting the survey completeness to an angular diameter distance 3 Mpc given by Figure 5 which is dominated by the non-overlapping nature of the flanking fields.

$10^{14}\,\mathrm{cm^{-2}}$ are strongly correlated with galaxies (Paper II), the gas may be predominantly located in the local environment of these galaxies as opposed to individual halos.

Finally, the identification of this O VI absorber with a single galactic halo is an important result in light of cosmological models of O VI gas. We emphasize that this O VI absorber has one of the largest equivalent widths at extragalactic distance. Cosmological simulations suggest that absorbers with large equivalent widths are the most likely to be collisionally ionized and also related to large-scale structures (Davé et al. 2001). In this case, however, the gas appears related to an individual galactic halo and therefore bears greater resemblance to the O VI gas observed in the halo of the Milky Way (Sembach et al. 2003). It will be very valuable to examine the galactic environment of the strongest O VI absorbers and perform quantitative comparisons with simulations.

5.3. $N_{\mathrm{HI}} > 10^{14}\,\mathrm{cm^{-2}}$ Absorbers Without Detected Metal-Lines

Before discussing the trends in the galactic environments of the metal-line absorbers, consider the environment of the absorbers with comparable N_{HI} but without detected metal-lines. Figure 9 presents a summary of the galactic environment of the non-metal systems with $N_{\mathrm{HI}} > 10^{14}\,\mathrm{cm^{-2}}$ from Williger et al. (2006). Examining the Figure, we note a picture qualitatively similar to the results for the metal-line systems. There are examples of dense galactic environments ($z = 0.0300, 0.2977, 0.4057$), absorbers potentially within individual galactic halos ($z = 0.2977, 0.3510$), and absorbers in very sparse environments ($z = 0.1825$) These results indicate that the cross-correlation observed between Lyα forest clouds with $N_{\mathrm{HI}} > 10^{14}\,\mathrm{cm^{-2}}$ and galaxies is not dominated by the metal-line systems.

5.4. Emerging Trends?

Considering the metal-line systems as a single class of absorbers, one might have expected similarities in their galactic environments. As Figure 7 qualitatively shows

(summarized in Table 3), the absorption systems exist near or within a wide range of galactic environments. There are examples where one can associate the absorber with the halo of a nearby bright galaxy, examples where there is no bright host yet a group or large-scale structure, and even an example ($z = 0.1825$) with no associated galaxies with $L \gtrsim L_*/2$. It is evident that metal-enriched gas generally associated with the IGM is located in a wide variety of environments at low redshift. A focus of our future work based on over 10 quasar fields will be to examine the incidence of O VI absorbers in each of these environments.

Although the PKS0405−123 sightline contains only a small sample of metal-line absorbers, one can search for emerging trends between their galactic environment and absorber properties. As a first step, we might separate the absorbers according to whether they are located in 'rich' or 'poor' galactic environments. To qualitatively assess the environment, we count the number of galaxies with $L > L_*/2$ and $|\Delta v| < 750\ \mathrm{km\,s^{-1}}$ within 3 Mpc of the sightline (Table 3). Under this definition, we classify the $z = 0.0918, 0.0965, 0.36$ absorbers as 'rich' ($N_{gal} > 4$) and the $z = 0.167, 0.1825$ absorbers as 'poor' ($N_{gal} < 3$). The survey is not sufficiently deep to consider the system at $z = 0.4951$. With these classifications, there is no obvious trend between galactic environment and absorber properties. The $z = 0.167$ and $z = 0.1825$ absorbers have very different characteristics (N_{HI} value, metallicity and ionization states). The rich-environment $z = 0.0965$ and $z = 0.3608$ absorbers also have dissimilar physical properties. In short, we find no trend between galactic environment and metallicity, N_{HI}, or ionization state, contrary to the strong correlation between $N(\mathrm{H\,I})$ and galaxy number density reported by Bowen et al. (2002). Given the small sample size (especially metal systems at $z < 0.1$ where $L < L_*/10$), our conclusions do not necessarily disagree with the findings of Stocke et al. (2006) who argue that the presence of metal-line systems is significantly correlated with galactic environment, but do not draw a conclusion about the properties of those systems with environment.

Examining Figure 7, it is apparent that the metal-line systems, which show a two magnitude spread in H I column density and metallicity, arise in regions with diverse galaxy density and distribution. For example, contrast the absorbers at $z = 0.0918$ and $z = 0.0965$ which exhibit similar H I column density and metal-line absorption. In both cases, there is a significant excess of galaxies observed at the redshift. In the case of $z = 0.0965$, the majority of galaxies lie within 1 Mpc of the absorber and very likely form a virialized group. In contrast, the galaxies associated with the $z = 0.0918$ absorber cover the entire field-of-view in a distribution suggesting a larger-scale, unvirialized structure (e.g. filament or sheet).

5.5. *The $z \sim 0.05$ Lyα Void*

Williger et al. (2006) have stressed that the sightline to PKS0405–123 exhibits no Lyα absorbers with $N_{\rm HI} > 10^{14}\,{\rm cm}^{-2}$ between $0.0320 < z < 0.0814$. They also have argued that the probability of this occurrence from a random redshift distribution is $P < 0.0004$. Given the correlation between strong absorbers and galaxies (Chen et al. 2005), one might expect a similar void in galaxies in this redshift interval. In the inner $10'$ minute field, we identify four galaxies with redshift $0.0320 < z < 0.0814$ at redshift: $z_{gal} =.043$ (ID 2716), 0.0668 (ID 2999), 0.0767 (ID 1463), 0.0770 (ID 993). Adopting the SDSS r^* luminosity function (Blanton et al. 2005), we predict 7.4 ± 3.2 galaxies in the volume subtended by a $10'$ radius where the uncertainty includes the effects of galaxy clustering (Connolly et al. 2002). Therefore, the number of observed galaxies is below the expected central value but well within the expected scatter.

6. SUMMARY

We summarize the principal results of this paper as follows:

- We presented the results of a galaxy redshift survey performed with the WFCCD spectrometer of the field surrounding PKS0405–123. The survey is nearly complete to $R = 20$ mag within a radius of $10'$. The Survey is supplemented by flanking fields covering $\approx 1\square^\circ$ to $R = 19.5$ mag. All of the galaxy spectra are publically available at http://www.ucolick.org/~xavier/WFCCDOVI/.

- We examined the galactic environment of the metal-line absorption systems identified along the sightline to PKS0405–123, all but one of which show O VI absorption. The systems arise within or near regions of the universe with a wide range of galactic environments including individual galactic halos, galaxy groups, filamentary-like structures, and regions devoid of bright galaxies. This suggests that metal-enrichment occurs in galaxies with a wide range of luminosity and environment.

- For the sightline to PKS0405–123, there is no significant difference in the galactic environment of $N_{\rm HI} > 10^{14}\,{\rm cm}^{-2}$ absorbers with or without metal-lines. If this holds with larger samples, it would suggest that metal-enrichment is a stochastic process with little dependence on galactic environment.

- In future papers, we will increase the sample size of sightlines by nearly an order of magnitude. Particular emphasis will be placed on studying the galactic environment of low redshift, O VI absorbers.

REFERENCES

Adelberger, K.L., Steidel, C.C., Shapley, A.E., & Pettini, M. 2003, ApJ, 584, 45
Aguirre, A., Hernquist, L., Schaye, J., Katz, N., Weinberg, D.H., & Gardner, J. 2001, ApJ, 561, 521
Bergeron, J. 1988, Large Scale Structures of the Universe, ed. J. Audouze, M.-C. Pelletan, & S. Szalay (Dordrecht: Kluwer Academic Publishers), p. 343
Bertin, E. Mellier, Y., Radovich, M., Missonnier, G., Didelon, P., & Morin, B. 2002, ASP Conf. Proc. v. 281, ed. D. Handley (San Fransisco: Astronomical Society of the Pacific), p. 228
Blanton, M. R., Eisenstein, D.; Hogg, D. W., Schlegel, D. J., & Brinkmann, J. 2005, ApJ, 629, 143
Bowen, D.V., Pettini, M., & Blades, J.C. 2002, ApJ, 580, 169
Cen, R. & Ostriker, J.P. 1999, ApJ, 514, 1
Chen, H.-W. & Prochaska, J.X. 2000, ApJ, 543, L9
Chen, H.-W., Lanzetta, K. M., & Webb, J.K. 2001, ApJ, 556, 158
Chen, X., Weinberg, D.H., Katz, N., & Davé, R. 2003, ApJ, 594, 42
Chen, H.-W., Prochaska, J.X., Weiner, B.J., Mulchaey, J.S., & Williger, G.M. 2005, ApJ, 629, 25L (Paper II)
Connolly, A.J. et al. 2002, ApJ, 579, 42
Danforth, C.W., & Shull, J.M. 2005, ApJ, 624, 555
Davé, R. & Tripp, T.M. 2001, ApJ, 553, 528
Davé, R., Cen, R., Ostriker, J.P., Bryan, G.L., Hernquist, L., Katz, N., Weinberg, D.H., Norman, M., & O'Shea, B. 2001, ApJ, 552, 473
Fukugita, M., Hogan, C.J, Peebles, P.J.E. 1998, Nature, 503, 518
Gnedin, N.Y. & Ostriker, J.P. 1997, ApJ, 486, 581
Grogin, N.A., & Geller, M.J. 1998, ApJ, 505, 506
Haardt, F. & Madau, P. 1996, ApJ, 461, 20
Haardt, F. & Madau, P. 1996, ApJ, 461, 20
Helsdon, S. F., & Ponman, T. J. 2000, MNRAS, 315, 933
Henry, R.B.C., Edmunds, M.G., & Köppen, J. 2000, ApJ, 541, 660
Impey, C. D., Petry, C. E., & Flint, K. P. 1999, ApJ, 524, 536
Jannuzi, B.T., et al. 1998, ApJS, 118, 1
Kennicutt, R.C., Jr. 1992, ApJ, 38, 310
Lanzetta, K.M. 1993, in The Environment and Evolution of Galaxies, ed. J.M. Shull & H.A. Thronson, Jr. (Boston: Kluwer Academic Publishers), p. 237
Lanzetta, K.M., Webb, J.K., & Barcons, X. 1996, ApJ, 456, 17
Lu, L., Sargent, W.L.W., Barlow, T.A., Churchill, C.W., & Vogt, S. 1996, ApJS, 107, 475
Morris, S.L., Weymann, R.J., Dressler, A., McCarthy, P.J., Smith, B.A., Terrile, R.J., Giovanellit, R., & Irwin, R.M. 1993, ApJ, 419, 524
Mulchaey, J.S., Mushotzky, R.F, Burstein, D., & Davis, D.S. 1996, ApJ, 456, 5L
Mulchaey, J. S., Davis, D. S., Mushotzky, R. F., & Burstein, D. 2003, ApJS, 145, 39
Penton, S.V., Stocke, J.T., & Shull, J.M. 2002, ApJ, 2002, 565, 720
Penton, S.V., Stocke, J.T., & Shull, J.M. 2004, ApJ, 2004, 152, 29
Prochaska, J.X., Chen, H.-W., Howk, J.C., Weiner, B.J., & Mulchaey J. S. 2004, ApJ, 617, 718 (Paper I)
Savage, B.D., Tripp, T., & Lu, L. 1998, ApJ, 115, 436
Savage, B.D., Sembach, K.R., Tripp, T., & Richter, P. 2002, ApJ, 564, 631
Scott, J., Bechtold, J., Morita, M., Dobrzycki, A., & Kulkarni, V.P. 2002, ApJ, 571, 665
Sembach, K.R., Wakker, B.P., Savage, B.D., Richter, P., Meade, M., Shull, J.M., Jenkins, E.B., Sonneborn, G., & Moos, H.W. 2003, ApJS, 146, 165
Sembach, K.R., Tripp, T.M., Savage, B.D., & Richter, P. 2004, ApJS, 155, 351

Spinrad, H., Filippenko, A. V., Yee, H. K., Ellingson, E., Blades, J. C., Bahcall, J. N., Jannuzi, B. T., Bechtold, J., & Dobrzycki, A. 1993, AJ, 1993, 106, 1

Steidel, C.C. 1993, *The Environment and Evolution of Galaxies*, ed. J.M. Shull & H.A. Thronson, Jr., (Boston: Kluwer Academic Publishers), p. 263

Stocke, J., Penton, S.V., Danforth, C.W., Shull, J.M., Tumlinson, J., & McLin, K.M. 2006, ApJ, submitted (astro-ph/0509822)

Tripp, T. M., Lu, L., & Savage B.D. 1998, ApJ, 508, 200

Tripp, T. M., Savage B.D., Jenkins, E.B. 2000, ApJ, 534, L1

Tripp, T.M. et al. 2002, ApJ, 575, 697

Tumlinson, J., Shull, J.M., Giroux, M.L., & Stocke, J.T. 2005, ApJ, 620, 95

Weymann, R.J., Vogel, S.N., Veilleux, S., & Epps, H.W. 2001, ApJ, 561, 559

Williger, G.M., Heap, S.R., Weymann, R.J., Davé, R., Ellingson, E., Carswell, R.F., Tripp, T.M., & Jenkins, E.B. 2006, ApJ in press, (astro-ph/055586)

Zhang, Y., Anninos, P., Norman, M.L., & Meiksin A. 1997, ApJ, 485, 496